Mitochondrial dysfunctions trigger the calcium signaling-dependent fungal multidrug resistance

Yeqi Li[a], Yuanwei Zhang[a], Chi Zhang[a], Hongchen Wang[a], Xiaolei Wei[a], Peiying Chen[b], and Ling Lu[a,1]

[a]Jiangsu Key Laboratory for Microbes and Functional Genomics, College of Life Sciences, Nanjing Normal University, 210023 Nanjing, China; and [b]Department of Dermatology, Jinling Hospital, School of Medicine, Nanjing University, 210002 Nanjing, China

Edited by Jay C. Dunlap, Geisel School of Medicine at Dartmouth, Hanover, NH, and approved November 6, 2019 (received for review July 8, 2019)

Drug resistance in fungal pathogens has risen steadily over the past decades due to long-term azole therapy or triazole usage in agriculture. Modification of the drug target protein to prevent drug binding is a major recognized route to induce drug resistance. However, mechanisms for nondrug target-induced resistance remain only loosely defined. Here, we explore the molecular mechanisms of multidrug resistance resulted from an efficient adaptation strategy for survival in drug environments in the human pathogen *Aspergillus fumigatus*. We show that mutants conferring multidrug resistance are linked with mitochondrial dysfunction induced by defects in heme A biosynthesis. Comparison of the gene expression profiles between the drug-resistant mutants and the parental wild-type strain shows that multidrug-resistant transporters, chitin synthases, and calcium-signaling-related genes are significantly up-regulated, while scavenging mitochondrial reactive oxygen species (ROS)-related genes are significantly down-regulated. The up-regulated-expression genes share consensus calcium-dependent serine threonine phosphatase-dependent response elements (the binding sites of calcium-signaling transcription factor CrzA). Accordingly, drug-resistant mutants show enhanced cytosolic Ca^{2+} transients and persistent nuclear localization of CrzA. In comparison, calcium chelators significantly restore drug susceptibility and increase azole efficacy either in laboratory-derived or in clinic-isolated *A. fumigatus* strains. Thus, the mitochondrial dysfunction as a fitness cost can trigger calcium signaling and, therefore, globally up-regulate a series of embedding calcineurin-dependent–response-element genes, leading to antifungal resistance. These findings illuminate how fitness cost affects drug resistance and suggest that disruption of calcium signaling might be a promising therapeutic strategy to fight against nondrug target-induced drug resistance.

drug resistance | fungi | *Aspergillus fumigatus* | calcium signaling | mitochondrial dysfunctions

Invasive fungal infections have risen steadily in recent decades due to the increasing number of immunocompromised patients and limited treatment options (1–3). Azoles are recommended as the first-line medicine for the primary treatment of fungal infectious diseases because of less side effects (4, 5). However, the steady rise of drug resistance in fungal pathogens is becoming a serious problem due to the fact that new antifungal drugs are difficult to be discovered (4, 5). Previous studies identified there were 3 major azole resistance mechanisms in fungal pathogens: changes in the drug target Cyp51, activation of drug efflux pumps, and induction of cellular stress responses (6–13). For the drug pumps which have been identified to be involved in drug resistance, there are, at least, 2 types of fungal drug efflux pumps: the ATP-binding cassette (ABC) transporters and the major facilitators superfamily (MFS) for which both are able to transport antifungal drugs out of the cell (11, 14, 15). Currently, it is known that drug efflux processes dominate the azole resistance whereas drug-target Cyp51 mutations are less important in yeast-type fungal pathogens *Candida albicans* (16). However, the most common mechanism of resistance to azole antifungals observed in the fungal pathogen *A. fumigatus*, one of the primary airborne ascomycete fungal pathogens and allergens, is linked to Cyp51A mutation which then results in the decreasing affinity of azoles for the Cyp51A protein, inducing resistance to multiple types of azoles (6, 7, 17). In addition, some mutations located in the promoter of *cyp51A* caused the overexpression of this gene and led to the azole resistance (12). Notably, there are a growing number of *A. fumigatus* isolates with non-*cyp51A* mutations that show azole resistance for unknown reasons (18, 19). It was hypothesized that the fungistatic activity of azoles against *A. fumigatus* (rather than fungicidal) could promote the selection of resistant strains (20, 21). Therefore, cotargeting the drug targets with fungal stress response regulators could be a promising strategy to enhance the efficacy of established antifungals and improve clinical outcomes (22). Moreover, nonantifungal compounds, such as the immunosuppressive drugs cyclosporine A (CsA), tacrolimus (FK506), and the heart-antiarrhythmic agent amiodarone with calcium channel blocker-like actions exhibit antifungal activity alone or in combination with antifungal drugs (23, 24). Notably, both CsA and FK506 are inhibitors of a highly conserved Ca^{2+}/calmodulin-dependent serine/threonine protein phosphatase, calcineurin, which is required for survival in membrane stress conditions induced by azoles (25). Moreover, fungal pathogens are able to respond to drug-induced stress by activating intracellular-signaling pathways (26). Of these, calcium signaling is involved in the antifungal-induced stress response, such as itraconazole (ITC), which is able to induce the $[Ca^{2+}]_c$

Significance

Millions of people with weakened immune systems are at a higher risk of developing different types of aspergillosis, whereas azole antifungals are the bedrock of therapy for these fungal infected diseases. The steady rise of drug resistance is becoming a serious problem, and thus, the understanding of azole resistance mechanisms could reveal novel approaches to restore the first-line azole efficacy. Here, we demonstrate that the mitochondrial dysfunction is able to activate calcium signaling and increase the expression of drug efflux pumps and chitin synthases, leading to the resistance of drugs. Findings suggest that these drug resistance mechanisms may exist in other pathogens, and disruption of calcium signaling is a promising approach to improve azole efficacy.

Author contributions: Y.L., C.Z., and L.L. designed research; Y.L., H.W., X.W., and P.C. performed research; C.Z. and L.L. contributed new reagents/analytic tools; Y.L., Y.Z., and L.L. analyzed data; and Y.L., Y.Z., and L.L. wrote the paper.

The authors declare no competing interest.

This article is a PNAS Direct Submission.

Data deposition: The data reported in this paper have been deposited in the Sequence Read Archive (SRI) database, https://www.ncbi.nlm.nih.gov/sra (accession nos. SRR10168714–SRR10168719).

See online for related content such as Commentaries.

[1]To whom correspondence may be addressed. Email: linglu@njnu.edu.cn.

This article contains supporting information online at https://www.pnas.org/lookup/suppl/doi:10.1073/pnas.1911560116/-/DCSupplemental.

First published December 6, 2019.

increasing sharply, but the addition of the calcium chelator almost blocks the calcium influx responses (13, 27).

Mitochondria not only are essential intracellular organelles for energy production, but also can sequester and release Ca^{2+} as a dynamic Ca^{2+} store (28). In yeast, cytochrome *c* oxidase (COX), the terminal enzyme of the electron transport chain, is a multimeric protein complex composed of 11 subunits (29). Cox10p plays a critical role in the mitochondrial heme biosynthetic pathway by catalyzing the conversion of heme B to heme O followed by Cox15p converted to heme A which presents a cofactor required for the stability and folding for the Cox1 subunit (30, 31). Deficiencies in the COX complex could cause the mitochondrial dysfunction (31). Moreover, the mitochondrial dysfunction can initiate a mitochondrial-nuclear cross talk which contributes to drug resistance in fungi (32, 33). We previously identified that one isolate carries a mutation in *cyp51A*, whereas all others have the wild-type *cyp51A* gene among a total of 105 isolated *A. fumigatus* resistant colonies (19). Furthermore, we found that this non-*cyp51A* mutation isolate has a Cox10 mutation (R243Q substitution) that contributes to azole resistance, but no molecular mechanism was addressed yet. In this study, we uncovered that the mitochondrial dysfunction was able to activate Ca^{2+} signaling and then to up-regulate a series of embedding calcineurin-dependent–response-element drug transporters for fungal survival against antifungals for these non-*cyp51A* resistant isolates.

Results

Defected Cox10 or Cox15 Causes Mitochondrial Dysfunction as Well as Reduced Growth and Virulence but Results in Enhanced Multidrug Resistance. To gain insight into how Cox10 is involved in azole susceptibility, we made 2 site-directed mutations E230A and D234A according to the conserved glutamic acid aspartic acid-rich motif (E-, D-rich motifs) embedded in Cox10 homologs. Mutations E230A, D234A, and the aforementioned resistant mutation R243Q, were all predicted to be located in the active center of the Cox10 enzyme. As a control, another mutation H331A was putatively located outside of the enzyme catalytic binding motif. Sequence alignments, phylogenetic analysis, and 3D model prediction showed that all of these amino acids were highly conserved (Fig. 1 *A* and *B* and *SI Appendix*, Fig. S1 *A* and *B*). As shown in Fig. 1*C* and *SI Appendix*, Fig. S1*C*, under the normal culture condition, the D234A mutation strain showed the sickest colony phenotype, and the R243Q mutant had a slightly reduced radial growth and conidiation. In comparison, mutation strains E230A and H331A displayed almost no detectable colony difference compared to that of the parental wild-type strain (Fig. 1*C* and *SI Appendix*, Fig. S1*C*). To further test the functions of these mutations in vivo, we analyzed the virulence potential of mutants in the wax moth *Galleria mellonella*. In the insect model, D234A showed the highest survival rate whereas R243Q resulted in a second higher survival rate of *G. mellonella* larvae compared to the parental wild-type strain ($P = 0.0001$ and $P < 0.0001$) (Fig. 1*D*). In comparison, mutation strains E230A and H331A exhibited a similar virulence potential to that of the parental wild-type strain (Fig. 1*D*). These data suggest that in vitro colony growth defects induced by dysfunction of Cox10 are underlined with reduced survival rates in the host insect model. However, after addition of ITC to the medium, the D234A and R243Q mutants displayed relatively robust colony growth with enhanced drug resistance, while the E230A mutant showed much less drug resistance (if any) compared to the H331A mutation and the parental wild-type strains, which were susceptible to the azole ITC showing almost completely abolished colony growth (Fig. 1*C*). This indicates that site-directed mutants with growth defects also displayed significantly increased azole antifungal resistance, suggesting the underlined link between Cox10 dysfunction and drug resistance. To further test whether these related mutants were cross-resistant to other antifungals, we used a standard broth-based microdilution method to assess clinically used antifungals including azoles, allylamines, and echinocandins. The overall minimal inhibitory concentrations (MICs) of voriconazole and terbinafine and the minimal effective concentrations (MECs) of caspofungin were listed in *SI Appendix*, Table S1. Mutants D234A and R243Q showed significant resistance to voriconazole, terbinafine, and caspofungin compared to the parental wild-type strain, H331A, and E230A, suggesting that the defective colony growth of Cox10 was consistently linked to multidrug resistance in *A. fumigatus*. To explore the relationship between Cox10 and drug resistance, a *cox10* deletion mutant was made (*SI Appendix*, Fig. S2*A*). As predicted, the *cox10* null mutant displayed remarkable colony-growth defects but with significantly increased azole resistance compared to the parental wild-type strain (Fig. 1*E* and *SI Appendix*, Fig. S2*B*). These growth defects and azole resistance were completely cured by reintegration of the *cox10* gene (strain $cox10^{C}$), which verifies the accuracy of the genetic manipulation (Fig. 1*E* and *SI Appendix*, Fig. S1*D*). Previous studies indicated that the major conserved function of Cox10 is involved in heme A biosynthesis which is required for stability and folding of the core subunit Cox1 of cytochrome *c* oxidase (29). In that pathway, Cox15 is a downstream enzyme that also plays a crucial role in heme A biosynthesis as Cox10 (34). Next, we wondered whether these drug resistance phenotypes were induced specifically by loss of Cox10 or due to the absence of heme A. We then constructed a Cox15 full-length deletion mutant (*SI Appendix*, Fig. S2*A*). As shown in Fig. 1*E* and *SI Appendix*, Fig. S1*D*, the *cox15* null mutant exhibited comparable phenotypes having the colony-growth defect and the multidrug resistance which was similar to those of the *cox10* mutant while the complemented strain ($cox15^{C}$) recovered these phenotypes to those of the parental wild-type strain. Through the analysis of heme composition by HPLC, the peak of putative heme A in the *cox10* and *cox15* deletion strains was undetectable compared to the parental wild-type and complemented strains (*SI Appendix*, Fig. S2*C*). Thus, these data collectively indicate that both defects of Cox10 and Cox15 conferred multidrug resistance might be linked with the heme A biosynthesis defect in *A. fumigatus*. Moreover, the contents of extracted ITC from hyphal cells were examined as shown in Fig. 1*F*, the *cox10* and *cox15* deletion strains had markedly (almost 5-fold) lower intracellular retentions of ITC compared to that of the parental wild-type and the complemental strains. These data suggest that the loss of *cox10* and *cox15* resulted in the drug resistance might be due to decreased cytosolic drug retentions. To further gain insight into Cox10 functions, we next labeled Cox10 at the C terminus with GFP and found that *Af*Cox10 was mainly colocalized with a mitotracker, indicating that Cox10 is a mitochondria-localized protein (*SI Appendix*, Fig. S2*D*). Thus, we further tested whether *cox10* related mutants could affect mitochondrial functions. As shown in Fig. 1*G*, deletions of *cox10* and *cox15* showed nonfermentable carbon source colony defects in a defined minimal medium (MM) supplemented by glycerol or ethanol as a sole carbon source compared with the robust hyphal growth and conidiation of the parental wild-type and complemental strains. These data suggest that loss of function of *cox10* or *cox15* could cause mitochondrial dysfunction. Since rhodamine 123 is known to be transported by certain drug membrane transporters and commonly used as a probe to test the mitochondrial membrane potential (35), we next analyzed the absorption of rhodamine 123 by FACS and showed that the *cox10* and *cox15* deletion strains also displayed reduced mitochondrial membrane potential activities (Fig. 1*H*), further indicating that mitochondrial-localized Cox10 is required for the usage of nonfermentable carbon sources and the maintenance of mitochondrial membrane potential.

Cox10 Mutations Induce Up-Regulation of a Series of Calcium-Dependent Serine-Threonine Phosphatase-Dependent Response Element Genes Including Multidrug Resistance Related Transport and Chitin Synthase Genes. To verify the molecular mechanism of drug resistance in *cox10*-related mutants, the whole-genome transcript profiles were comparatively analyzed in the R243Q

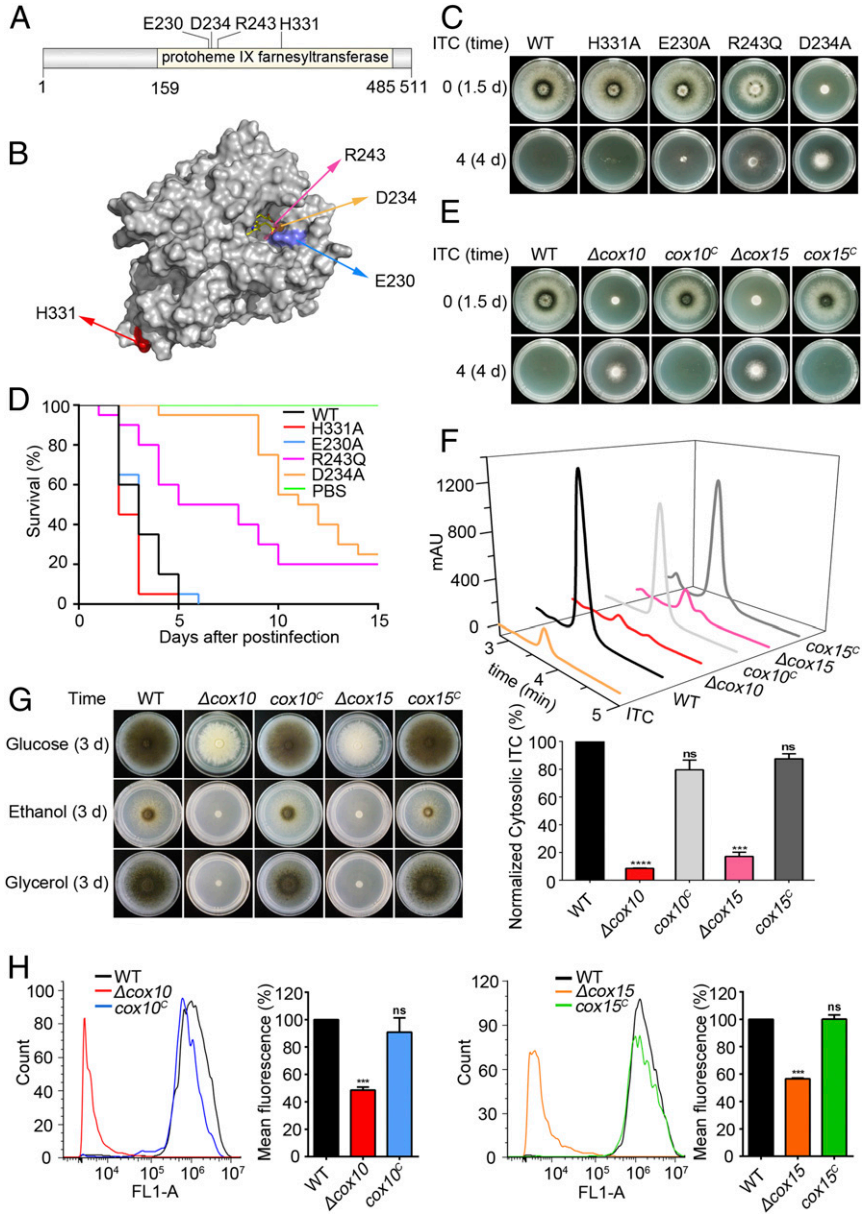

Fig. 1. Defected Cox10/Cox15 causes mitochondrial dysfunction as well as reduced growth and virulence but results in enhanced multidrug resistance. (*A* and *B*) The conserved site-directed Cox10 sites were predicted by domain alignments and 3D model prediction. (*C*) Phenotypes of the indicated strains on MM at 37 °C for 1.5 d or on MM with ITC supplementation (4 μg/mL) for 4 d. (*D*) Survival curves of *G. mellonella* larvae infected with the parental wild-type strain and Cox10 mutants. PBS-injected larvae served as controls. (*E*) Phenotypes of the indicated strains on MM at 37 °C for 1.5 d or on MM with ITC supplementation (4 μg/mL) for 4 d. (*F*) The intracellular ITC concentrations in the indicated strains analyzed by HPLC. mAU refers to milliabsorbance units. Normalized quantification and comparison of the ITC contents in mutants and the parental wild-type strain. (*G*) Colony phenotypes of indicated strains on MM containing glucose, ethanol, or glycerol, respectively, as a sole carbon source at 37 °C for 3 d. (*H*) Accumulated rhodamine 123 detection by fluorescence-activated cell sorting (FACS) in indicated strains. FL1-A on the X axis represented the relative fluorescence intensity value. The fluorescence intensity was normalized to that of the parental strain under the same condition. Statistical significance was determined using a 2-tailed *t* test. ns, not significant; ***$P < 0.001$; ****$P < 0.0001$.

mutation and *cox10* null mutants compared to that of the parental wild-type strain (Dataset S1). The Venn analysis indicated that the *cox10* null and R243Q mutants had 192 overlapping differentially expressed genes ($P \leq 0.05$, $|\log_2 FC| \geq 4$) compared to that of the parental wild-type strain (Fig. 2*A*). In the ranking of the genes with the most up-regulated expression levels ($P \leq 0.05$, $|\log_2 FC| \geq 2$), the multiple putative ABC transporter and the calcium channel genes appeared (Fig. 2*B* and *SI Appendix*, Fig. S3 *B* and *C*). In contrast, there were many down-regulated genes for which catalases encoding genes *easC, catB*, and *cat2* were listed in *cox10* mutants compared to that of the parental wild-type strain (Table 1 and *SI Appendix*, Fig. S3*C*). A quantitative real-time PCR (qRT-PCR) in the additional biological replicate samples confirmed the differential expression of these genes as shown in Fig. 2*F* and *SI Appendix*, Fig. S4*A*, suggesting that the majority of these selected gene expression differences were consistent with those in the data set of RNA-seq. Interestingly, compared to its parental wild-type strain, the *cox10* null mutant displayed remarkable mRNA changes in the high-affinity Ca^{2+}-ATPase coding genes *pmcC* (120-fold), *pmcB* (60-fold), and *pmcA* (3-fold), the transmembrane transport coding gene *tpo3* (36-fold), the C2H2 finger domain protein coding gene

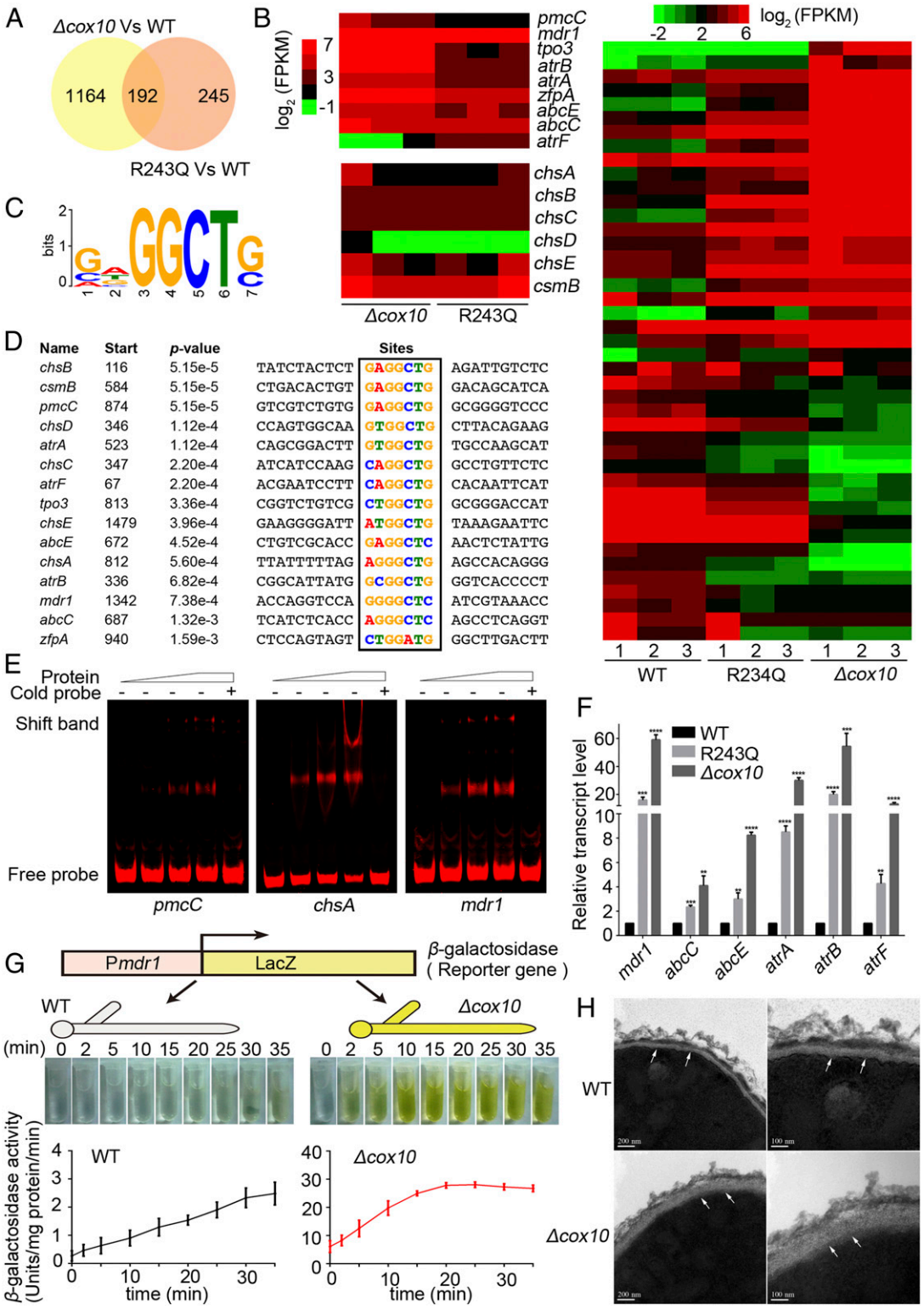

Fig. 2. Cox10 mutations induce the up-regulation of a series of CDRE genes including multidrug-resistance-related transports and chitin synthase genes. (*A–D*) RNA-seq analysis of the whole-genome transcript profiles in the *cox10* null mutants and R243Q mutation compared to that of the parental wild-type strain. (*A*) Venn diagram showed the overlap of differentially expressed genes in the *cox10* null mutants and the R243Q mutation strain compared to that of the parental wild-type strain. (*B*) A heat map comparison of the RNA-seq data in the *cox10*-related mutant compared to that of their parental wild-type strain. Colors represented changed $\log_2$ values of the ratio of RNA levels detected in the indicated mutant strains compared to those present in the parental wild-type strain. (*C* and *D*) Putative CDRE binding sequence alignment in promoters of indicated genes. (*E*) Electrophoretic mobility shift assays (EMSA) showed the in vitro binding of CrzA to Cy5-labeled promoter fragments of genes *pmcC*, *chsA*, and *mdr1*. Nonlabeled DNA fragments (cold probe) as competition assays. (*F* and *G*) The up-regulation of indicated multidrug-resistance-related transport genes were verified by qRT-PCR, and the transcript level of multidrug-resistant transport gene *mdr1* was confirmed by β-galactosidase activity assay. Statistical significance was determined using a 2-tailed *t* test. $^{**}P < 0.01$; $^{***}P < 0.001$; $^{****}P < 0.0001$. (*H*) The transmission electron microscope (TEM) images of the *cox10* null mutant and the parental wild-type strain. Arrows indicated the cell wall.

Table 1. Selected expression-changed genes which may contribute to drug resistance in *cox10* mutants

Gene name (*A. f* /*S. c*)	Gene ID	Description	Fold changes (log_2)	
			Δ*cox10*/WT	R243Q/WT
		Calcium-signaling/homeostasis related genes		
pmcC/*pmc1*	AFUB_087610	Calcium transporting ATPase (Pmc1)	10.10 ± 2.84	5.25 ± 2.47
tpo3/*tpo3*	AFUB_101650	Crz1 target, MFS multidrug transporter	7.89 ± 1.62	4.03 ± 0.77
zfpA/*ace2*	AFUB_082490	Crz1 target, C2H2 finger domain protein	3.34 ± 0.61	2.12 ± 0.35
pmcB/*pmc1*	AFUB_038470	Calcium-translocating P-type ATPase	2.85 ± 1.87	1.39 ± 0.42
mcuA	AFUB_067410	Conserved protein	1.15 ± 0.64	−0.22 ± 1.37
pmcA/*pmc1*	AFUB_010300	P-type calcium ATPase	0.91 ± 0.60	0.15 ± 0.54
		Multidrug transport related genes		
mdr1/*ste6*	AFUB_053630	ABC multidrug transporter Mdr1	7.46 ± 0.55	1.42 ± 1.72
atrB/*snq2*	AFUB_047000	ABC multidrug transporter, putative	6.40 ± 0.79	2.93 ± 0.69
atrA/*pdr15*	AFUB_041770	ABC multidrug transporter, putative	4.85 ± 0.66	3.04 ± 0.77
atrF/*snq2*	AFUB_093930	ABC drug exporter AtrF	2.72 ± 1.16	1.08 ± 0.04
abcE/*ste6*	AFUB_087060	ABC multidrug transporter, putative	2.55 ± 0.16	1.54 ± 0.59
abcC/*pdr15*	AFUB_013880	ABC transporter, putative	1.99 ± 0.63	1.09 ± 0.99
		Chitin synthase genes		
chsA/*chs1*	AFUB_018960	Putative class I chitin synthase	1.99 ± 0.59	1.06 ± 0.05
chsE/*chs3*	AFUB_029080	Putative class V chitin synthase	1.71 ± 0.91	1.39 ± 0.19
csmB/*chs3*	AFUB_029070	Putative chitin synthase	0.94 ± 0.46	0.56 ± 0.26
chsD/*chs3*	AFUB_012070	Putative chitin synthase-like gene	0.86 ± 1.04	1.05 ± 0.74
chsC/*chs2*	AFUB_049230	Putative class III chitin synthase	0.82 ± 0.61	0.70 ± 0.22
		Catalases		
easC/*cta1*	AFUB_033720	Catalase easC	−6.29 ± 1.56	−0.07 ± 0.33
catB/*cta1*	AFUB_046060	Mycelial catalase Cat1	−3.54 ± 1.77	−2.70 ± 0.83
cat2/*ccp1*	AFUB_084930	Bifunctional catalase-peroxidase Cat2	−1.35 ± 1.17	−0.21 ± 0.28

A. f, *A. fumigatus*; *S. c*, *S. cerevisiae*; R243Q, $Cox10^{R243Q}$.

zfpA (8-fold), and the mitochondrial calcium uniporter gene *mcuA* (9-fold) (*SI Appendix*, Fig. S4*A*). Notably, the putative ABC transporter genes *mdr1*, *atrA, atrB, atrF, abcC*, and *abcE* all showed remarkable up-regulation in both the R243Q mutation and the *cox10* deletion strain compared to the parental wild-type strain (Fig. 2*F*). We next used *mdr1*, which is a key drug-resistance-related gene by actively extruding diverse drugs out of the intracellular environment (15, 36) as a representative to further visualize the differential expression between the mutant and the parental wild-type strain by fusing the *mdr1* promoter with a bacterial *lacZ* reporter gene. As shown in Fig. 2*G*, the *β*-galactosidase activity increased 10-fold with a yellow color in samples extracted from the *cox10* null mutant compared with samples from the parental wild-type strain, indicating that the promoter of *mdr1* was truly more active in the *cox10* null mutant. To test whether *mdr1* was involved in drug resistance, the *mdr1* deletion was then constructed in both the parental wild-type and the *cox10* deletion strains. As shown in *SI Appendix*, Fig. S5*A*, lack of *mdr1* largely reduced drug resistance in the *cox10* deletion background strain especially under the high concentration of azoles, implied that the drug resistance in the *cox10* mutant is related to the multidrug transport gene *mdr1*. In addition, from the expression-changed gene list, we found that a series of the chitin synthase genes were included (Fig. 2*B* and *SI Appendix*, Fig. S6*C*), we wondered whether they may affect cell-wall phenotypes. High-performance ionic chromatography coupled to pulse amperometry detection identified that the relative monosaccharide contents of chitin had marked increases in the *cox10* mutants (*SI Appendix*, Fig. S6*A*) and the *cox15* null mutant (*SI Appendix*, Fig. S6*B*), and the *cox10* mutants displayed more resistance to the cell-wall damage agents calcofluor white and congo red compared to that of the parental wild-type strain (*SI Appendix*, Fig. S6*D*). In agreement, TEM showed a much thicker cell wall in the *cox10* deletion strain, accompanied with a longer time to produce protoplasts by the cell-wall enzyme digestion than that of the parental wild-type strain (Fig. 2*H* and *SI Appendix*, Fig. S6 *E* and *F*). These data suggest that changed expression of the chitin synthase genes in the *cox10* mutants underlies abnormally related cellular phenotypes. Most interestingly, the differentially expressed genes shared the consensus CrzA-binding calcium-dependent serine-threonine phosphatase-dependent response element (CDRE) sites in their promoters by a software MEME analysis (Fig. 2 *C* and *D*). To investigate whether *A. fumigatus* CrzA could directly interact with the predicted CDRE motif, we expressed CrzA in *Escherichia coli* and analyzed protein-DNA interaction (*SI Appendix*, Fig. S5*B*). As shown in Fig. 2*E* and *SI Appendix*, Fig. S5*C*, CrzA was able to bind with promoter fragments of *pmcC*, *chsA*, *mdr1*, *chsC*, *abcE*, and *atrB* genes but not with that of *atrF* in EMSA. Excess of unlabeled DNA fragments (cold probe) blocked the interaction of CrzA within the promoter fragments, underlining the specificity of the protein/DNA interaction. These data imply that the *cox10* related mutants may systematically induce the up-regulation of transcription factor-CrzA targeted genes.

Loss of Function in Cox10 Results in Reduced Mitochondrial Ca^{2+} Response Amplitude and Enhanced Cytosolic Ca^{2+} Transients. Since mitochondria play essential roles in buffering transient increases in cytosolic free calcium in response to stress stimuli, Ca^{2+} uptake into mitochondria plays a central role in cell physiology by stimulating ATP production, shaping cytosolic Ca^{2+} transients, and regulating cell survival or death (28, 37, 38). Moreover, the aforementioned comparison of RNA-seq data between the *cox10* null mutant and its parental wild-type strain indicates that the calcium homeostasis-related genes had been markedly changed. Thus, we hypothesized that the mitochondrial dysfunction induced by defective *cox10* resulted in abnormal Ca^{2+} transients which may contribute to drug resistance. It has been identified that the bioluminescent apoaequorin system is an accuracy measurement method for intracellular calcium. Once bonded with free calcium, aequorin is converted into apoaequorin, carbon dioxide, and coelenteramide, and energy from this reaction is released as blue light which can be used to report

MICROBIOLOGY

$[Ca^{2+}]_c$ inside cells (39). Thus, we next constructed a mitochondrial targeted version of the Ca^{2+}-sensitive photoprotein-aequorin system to analyze the mitochondrial calcium transient which reflects the response to the extracellular environment. When treated with 0.1 M $CaCl_2$, the mitochondrial Ca^{2+} amplitude in the *cox10* deletion strain showed a reduction of 25 ± 4% in the peak value compared to that of the parental wild-type strain under the same detection condition (Fig. 3*A*). In agreement, site-directed mutants also displayed decreased $[Ca^{2+}]_{mt}$ amplitudes to some extent, while there was no significant change between the H331A mutant and the parental wild-type strain (Fig. 3*A*). In contrast, the cytoplasmic calcium $[Ca^{2+}]_c$ measurement indicated that *cox10* deletion, D234A, R243Q, and E230A but not H331A showed significantly increased amplitudes compared to that of the parental wild-type strain as shown in Fig. 3*B*. These data indicate that Cox10 may contribute to Ca^{2+} uptake into mitochondria and that defects in the putative active center of the putative farnesyltransferase Cox10 result in abnormal cellular calcium homeostasis.

Abnormal Cytoplasmic Ca^{2+} Transient Induced by Defects of Cox10 Causes a Persistent Nuclear Localization of CrzA Which Contributes to Drug Resistance. It has been reported that increased cytosolic Ca^{2+} normally binds the Ca^{2+} sensor protein calmodulin, subsequently activates the phosphatase calcineurin, and then dephosphorylates the transcription factor CrzA, leading to its nuclear translocation to regulate downstream targets (38, 40). We next wondered whether the abnormally elevated cytosolic Ca^{2+} transients in *cox10*-related mutants could cause localization changes in the transcription factor CrzA. As shown in Fig. 3*C* and *SI Appendix*, Fig. S7, when the parental wild-type strain was cultured in MM, CrzA-GFP was located in the cytoplasm. However, once stimulated by the addition of calcium, it clearly showed a nuclear localization pattern with the overlapped signal of nuclear (DAPI) staining (Fig. 3*C* and *SI Appendix*, Fig. S7). In comparison, the ITC treatment had a similar effect as that of the calcium addition for stimulating CrzA-GFP nuclear translocation (*SI Appendix*, Fig. S7). However, unlike this translocation style observed in the parental wild-type strain, CrzA-GFP in the majority of hyphal cells (~90%) in the *cox10* deletion mutant showed the persistent nuclear localization regardless of whether calcium was added (Fig. 3*C* and *SI Appendix*, Fig. S7). In contrast, addition of FK506, an inhibitor of calcineurin, completely abolished the nuclear localization of CrzA (*SI Appendix*, Fig. S7). In comparison, mutants D234A and R243Q displayed clear persistent nuclear localization, while E230A showed partial nuclear localization (if any) to some extent, but the H331A mutant still had a wild-type–like CrzA-GFP translocation pattern with cytoplasmic localization when cultured in normal medium without treatment with the calcium stimulus (*SI Appendix*, Fig. S8). These data suggest that enhanced cytoplasmic Ca^{2+} transients, induced by defects of Cox10, may cause persistent nuclear localization of CrzA which is dependent on the function of calcineurin. To further verify the tight link between CrzA and drug resistance, we made a conditionally expressed CrzA strain under the control of the promoter Tet on–off system in the background of the parental wild-type strain, the R243Q mutation, and the deletion strains, respectively, in which the expression of *crzA* was induced or repressed in the medium with or without doxycycline. As shown in *SI Appendix*, Fig. S9*A*, these conditional strains were successfully constructed. Interestingly, down-regulation of CrzA markedly decreased the expression of a series of tested multidrug-resistant transport genes, including *mdr1*, *atrB*, *atrF*, and *abcE* but not *atrA* or *abcC* in the *cox10* defective mutants (*SI Appendix*, Fig. S9*B*). In agreement, down-regulation of CrzA also inhibited the expression of tested chitin synthase genes *chsA*, *chsC*, *chsE*, and *csmB* but not *chsB* and *chsD* (*SI Appendix*, Fig. S9*B*). These data suggest that CrzA is required for the overexpression of major multidrug transport genes and most chitin synthase genes. Moreover, the HPLC assay further identified that down-regulation of CrzA in *cox10* defective mutants significantly recovered the abnormal low cytosolic itraconazole retention toward a wild-type level (Fig. 4*A*). These data suggest that overexpression of multidrug transport genes accompanied with reduced cytosolic ITC retention in *cox10* defective mutants is dependent on the expression of CrzA, which underlines a link between CrzA and drug resistance via the regulation of major multidrug transport genes expression.

As aforementioned, the *cox10*-related mutants had a consistent tendency for the abnormally enhanced cytoplasmic Ca^{2+} transients and the up-regulated expression of drug-resistance-related genes. To further identify whether the drug-resistance phenotype resulted from enhanced cytoplasmic Ca^{2+} transients, we then used a cell permeable and highly selective calcium chelator, 1,2-bis(*o*-aminophenoxy)ethane-*N*,*N*,*N*′,*N*′-tetraacetic acid tetrakis(acetoxymethyl ester) (BAPTA-AM), to chelate intracellular Ca^{2+}. In contrast to the persistent nuclear localization of CrzA induced by the loss of *cox10* function in the normal medium, the addition of BAPTA-AM strikingly prompted CrzA-GFP to the cytoplasmic localization as shown in Fig. 4*B* and *SI Appendix*, Fig. S10*A*. Coincidentally, BAPTA-AM also reduced the azole resistance of *cox10*-related mutants under liquid culture conditions (Fig. 4*C*). To further identify whether the cytosolic Ca^{2+} transient truly influences azole efficacy, we amended another extracellular Ca^{2+} chelator, BAPTA, to liquid media and tested the minimal inhibitory concentration to the antifungal ITC. As shown in *SI Appendix*, Fig. S9*C*, the azole resistance of *cox10*-related mutants was also significantly reduced by BAPTA. These data collectively imply that chelating intracellular Ca^{2+} or blocking the entrance of extracellular calcium is able to restore drug susceptibility to some extent and, thus, significantly increase azole efficacy. We then wondered whether other *A. fumigatus* azole-resistance isolates were linked to the enhanced cytoplasmic Ca^{2+} transients induced by defective mitochondrial function. We tested MIC values for 89 independent isolates obtained previously (19). Among the 34 mitochondrial-defective isolates which displayed nonfermentable carbon source colony growth defects and the reduced mitochondrial membrane potential (Fig. 5 *A* and *B* and *SI Appendix*, Figs. S11 and S12), 14 independent isolates had reduced MIC values by the addition of BAPTA-AM (*SI Appendix*, Table S2), indicating that approximately half of drug-resistant isolates with mitochondrial defects might be associated with enhanced cytoplasmic Ca^{2+} homeostasis. Moreover, we further tested the synergistic effects of the calcium chelator and ITC in 6 clinical isolates, and data were shown in *SI Appendix*, Fig. S10*B*, indicating that chelating intracellular Ca^{2+} was able to significantly increase the azole efficacy in these *A. fumigatus* clinic isolates. Taken together, these data collectively suggest that an enhanced cytosolic Ca^{2+} transient is one major reason for non-*cyp51A* drug resistance in *A. fumigatus* isolates.

Discussion

Resistance mutations are generally expected to come with a cost; in the absence of the antifungal drug, a resistant isolate has a lower fitness than wild-type isolates (20). However, under long-term drug treatment conditions, azole resistance is an efficient adaptation strategy of fungal pathogens in the human host or in the environment (20, 41). The fungus can use various strategies to overcome environmental stress factors, depending on its morphological state (42, 43). Increasing evidence from scientists and clinicians demonstrates that there are complicated and unknown drug resistance mechanisms besides the mutational modification of the azole target protein Cyp51A in fungal pathogens (9, 18). Our previous work identified a new mutation in the putative *A. fumigatus* farnesyltransferase Cox10 having no detectable change in the ergosterol level in a laboratory-derived ITC resistant isolate (19). More recently, whole-genome sequencing of non-Cyp51A azole-resistant *A. fumigatus* isolates from clinic and environment has identified 2 amino acid substitutions presenting in *Af*Cox10 (P17S and A423V), implying that

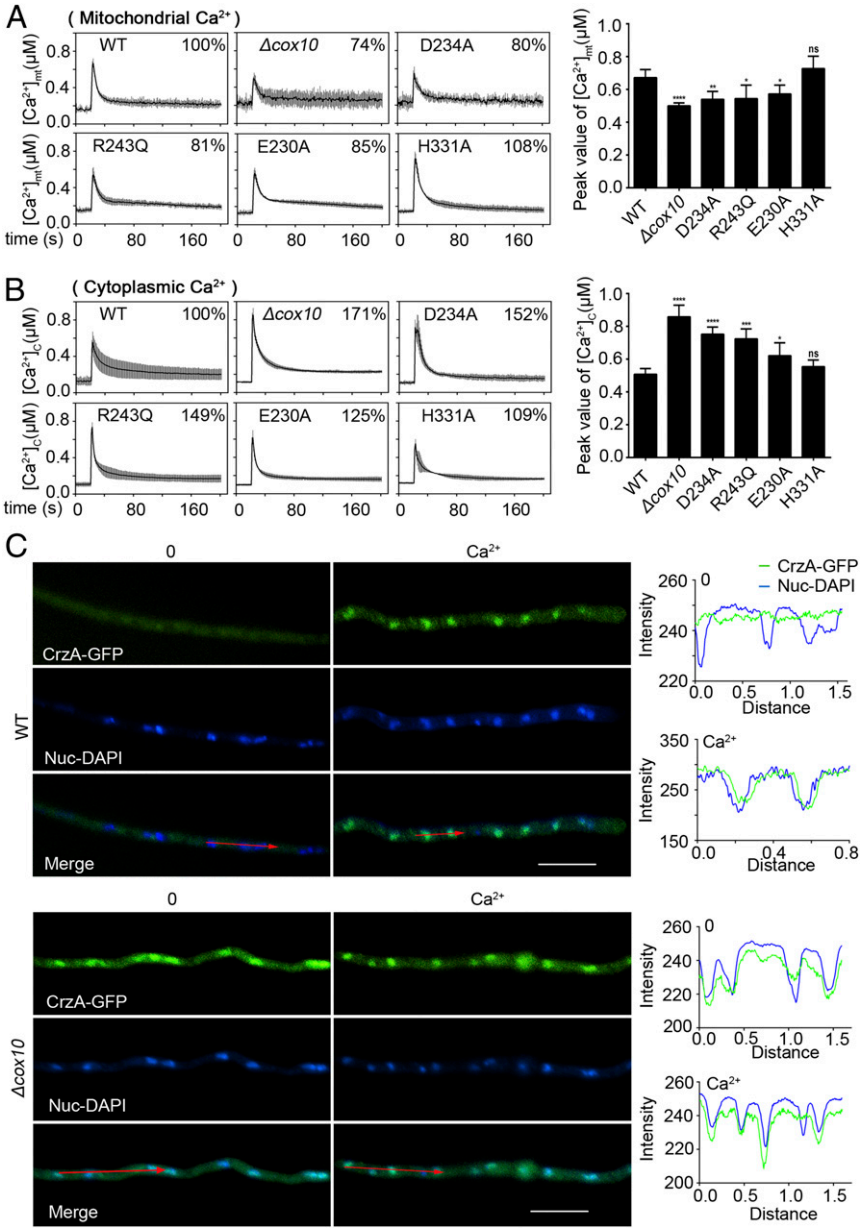

Fig. 3. Loss of function of Cox10 results in reduced mitochondrial Ca^{2+} sequestration and enhanced cytosolic Ca^{2+} transients. (*A*) Mitochondrial $[Ca^{2+}]_{mt}$ responses in the parental wild-type strain and the indicated *cox10* mutants following a stimulus of high external calcium (0.1 M $CaCl_2$). The bar graph showed the peak value of $[Ca^{2+}]_{mt}$ amplitude as percentages of that of the parental wild-type strain. (*B*) Cytosolic $[Ca^{2+}]_c$ responses in the parental wild-type strain and the indicated *cox10* mutants following a stimulus of high external calcium (0.1 M $CaCl_2$). The bar graph showed the peak value of $[Ca^{2+}]_c$ amplitude in mutants as percentages of that of the parental wild-type strain. Statistical significance was determined using a 2-tailed *t* test. ns, not significant; $*P < 0.05$; $**P < 0.01$; $***P < 0.001$; $****P < 0.0001$. (*C*) Epifluorescence microscopic images demonstrating the CrzA-GFP distribution under the untreated (*Left*) or treated conditions with Ca^{2+} (100 mM) for 15 min (*Right*) in the parental wild-type and Δ*cox10* strains, respectively. DAPI was a nuclear localization signal dye used to visualize the nucleus. The merged images of GFP and DAPI stainings showed nuclear localization of CrzA-GFP. The green line represented CrzA-GFP, and the blue line represented DAPI. (*Right*) Showing distribution patterns of CrzA-GFP and DAPI analyzed by the software Image J. Bars, 10 μm.

Cox10 mutation-induced azole-resistant isolates may exist in clinical and environmental conditions (44). In this study, we found that *cox10* mutants caused the enhanced multidrug resistance and reduced colony growth as well as decreased virulence in hosts. These data suggest that the Cox10 enzyme activity might be required for the normal fungal growth, while its partial loss of Cox10 function may be a compromise strategy for long-term survival in a drug environment. Moreover, we provide several lines of evidence demonstrating that reduced drug susceptibilities are not only limited to identified *cox10* mutations, but also result from the mitochondrial dysfunction. Therefore, we propose that there are 3 major possibilities leading to the drug resistance in these mitochondrial-defected mutants. First, the HPLC assay showed that *cox10*-related mutants had markedly decreased cytoplasmic ITC concentrations, implying that the efficacy of the drug efflux pump or the drug entrance route can be changed. In agreement with this deduction, RNA-seq, qPCR, and LacZ assays collectively verified a global overexpression of multidrug transport genes especially the drug efflux pump representative Mdr1. Second, overexpression of chitin synthase genes accompanied with much thicker cell walls in *cox10* mutants suggests that the drug resistance may also come

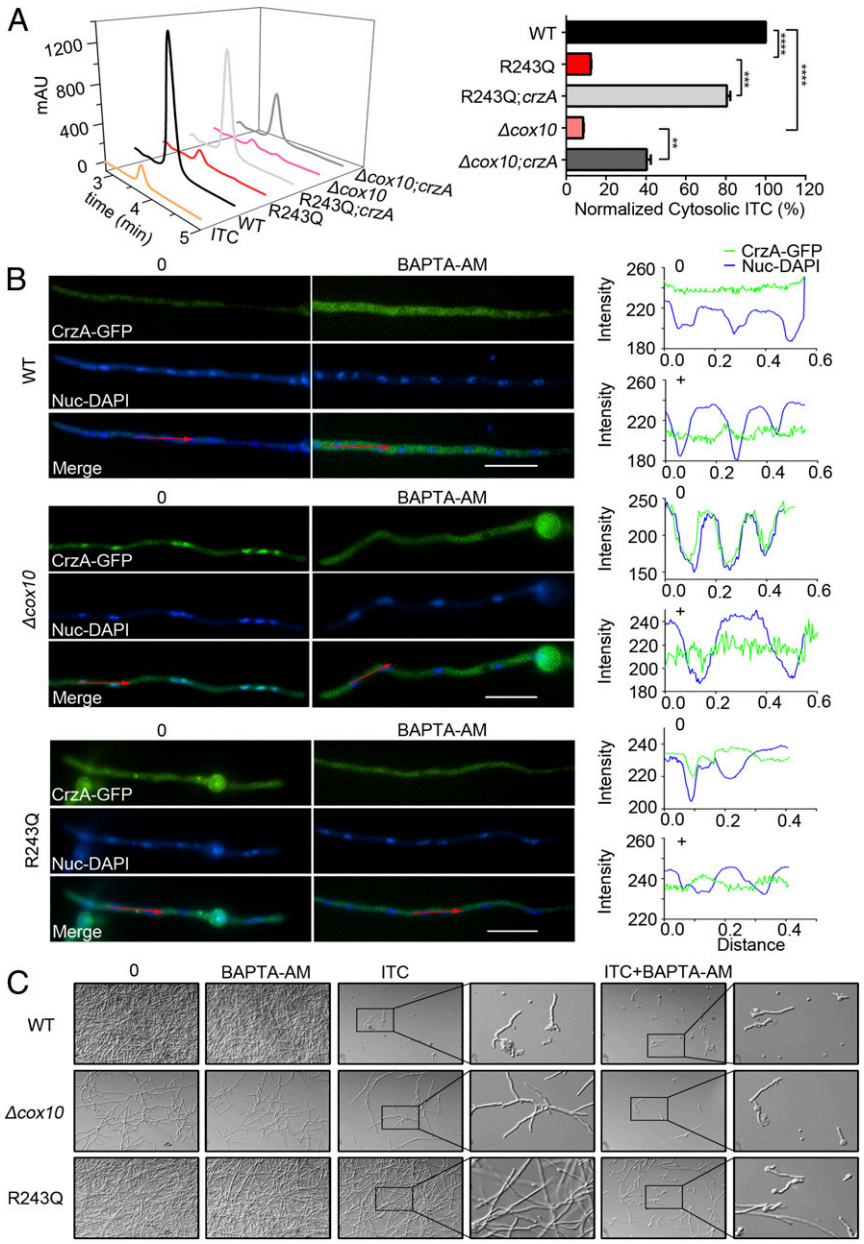

Fig. 4. Abnormal cytoplasmic Ca^{2+} transient induced by defects of Cox10 causes a persistent nuclear localization of CrzA which contributes to drug resistance. (*A*) Down-regulations of *crzA* in *cox10*-related mutants resulted in increased intracellular ITC concentrations detected by HPLC. mAU refers to milliabsorbance units. Normalized quantification and comparison of the ITC contents in mutants and the parental wild-type strain. Statistical significance was determined using a 2-tailed *t* test. $^{**}P < 0.01$; $^{***}P < 0.001$; $^{****}P < 0.0001$. (*B*) Fluorescence images of CrzA-GFP in mycelia under the untreated (*Left*) or treated conditions with 30 μg/mL BAPTA-AM for 30 min (*Right*) in indicated strains. The merged images of GFP and DAPI stainings showed that CrzA-GFP was localized in the cytoplasm when treated with BAPTA-AM. The green line represented CrzA-GFP, and the blue line represented DAPI. (*Right*) Showing distribution patterns of CrzA-GFP and DAPI analyzed by the software Image J. Bars, 10 μm. (*C*) Germlings and hyphal growth phenotypes in indicated strains under the liquid MM treated by BAPTA-AM (30 μg/mL), ITC (0.3 μg/mL) or ITC combined with BAPTA-AM at 37 °C for 1.5 d.

from less drug entrance than that of the parental wild-type strain. Third, since many lines of evidence indicate the drug efficacy is associated with the ROS burst in mitochondria (45–47), data for which down-regulation of catalase-encoding genes and less production of mitochondrially derived ROS in the mutants (*SI Appendix*, Fig. S4 *A* and *B*) also suggest that reduced ROS may, in part, contribute to the drug resistance.

Most interestingly, we found that the up-regulated genes, which may be related to drug resistance, share the CDRE motif in promoters. This information indicates that the *cox10* mutants may affect the cellular calcium-signaling pathway. In previous studies, it has been identified that the transcription factor CrzA was able to directly bind the promoters of chitin synthase genes and regulate the expression of these genes (48), but until now, there have not been any reports that the activation of calcium signaling could affect a series of multidrug transporters. In all eukaryotic cells, calcium is a second messenger that is involved in growth, development, secretion, transportation, and stress response (38). In fungi, upon stimulation by various external stresses, increased cytosolic Ca^{2+} first leads the Ca^{2+} sensor protein calmodulin to be activated through binding with calcium ions and subsequently activates the phosphatase calcineurin,

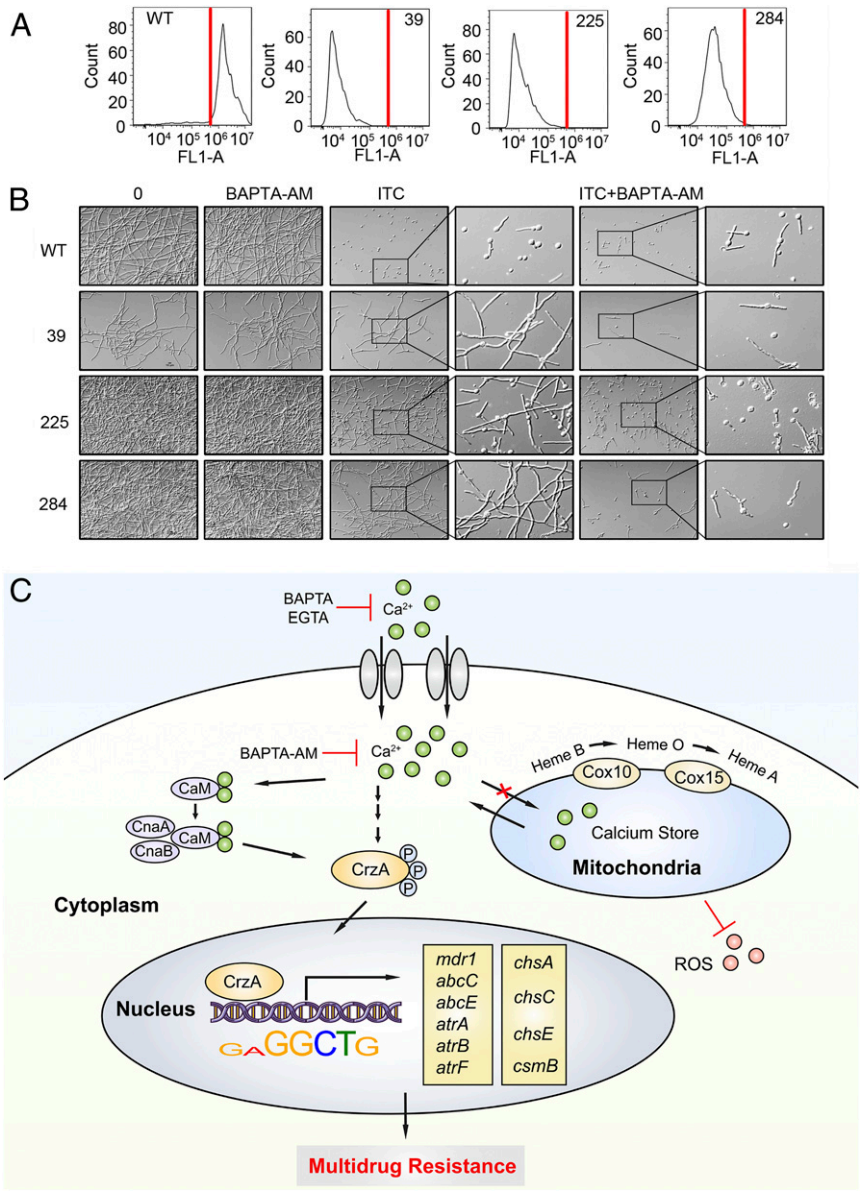

Fig. 5. The synergistic inhibitory effect of ITC with the calcium chelator BAPTA-AM for the hyphal growth in the mitochondrial membrane potential-defected *A. fumigatus* isolates. (*A*) The accumulated rhodamine 123 in strains detected by FACS showing the mitochondrial membrane potential. FL1-A on the X axis represented the relative fluorescence intensity value. (*B*) Hyphal phenotypes of laboratory-derived isolates No. 39, 225, and 284 strains under the liquid MM cultural condition treated by different reagents of BAPTA-AM (30 μg/mL), ITC (0.3 μg/mL), or both at 37 °C for 1.5 d. (*C*) A schematic showing how the calcium-signaling activation induced by the mitochondrial dysfunction in *cox10* mutants contributes to fungal drug resistance.

which then dephosphorylates the transcription factor CrzA/Crz1, leading to its nuclear translocation (25, 40). CrzA/Crz1 is then recruited to the nucleus where it transcriptionally regulates downstream signaling pathways to alleviate cellular stress and promote cell survival (40). Therefore, these data suggest that global up-regulation of CDRE genes might be due to activation of CrzA by its translocation to the nucleus. Accordingly, we found that, in the *cox10* mutants, CrzA was always localized in the nucleus regardless of calcium stimuli, suggesting that abnormal calcium homeostasis induced by the *cox10* mutants might be linked to this persistent nuclear localization of CrzA. Moreover, the EMSA experiment demonstrated that CrzA was truly capable of binding the predicted CDRE motifs in these up-regulated genes. In addition, down-regulated expression of CrzA significantly inhibited overexpression of *mdr1* and chitin synthase genes which coincides with partial rescue of the decreased cytosolic ITC retention. These results demonstrate that CrzA-regulated calcium signaling is involved in drug resistance in the *cox10* mutants. In fact, the *cox10* mutants truly had enhanced cytoplasmic calcium transients as well as reduced mitochondrial calcium levels, indicating that calcium homeostasis (cytoplasmic calcium buffer capacity) was changed in these *cox10*-related drug-resistant mutants. These data also suggest that the persistent nuclear localization of CrzA, which contributes to drug resistance, could result from abnormal cytoplasmic Ca^{2+} transients that might be due to the mitochondrial dysfunction in the calcium storage. Although increased intracellular Ca^{2+} (i.e., calcium transients) was found in the *cox10* mutant upon the addition of exogenous Ca^{2+}, the baseline level of intracellular Ca^{2+} (i.e., unstimulated) in the mutant was not detectably changed compared to that of the parental wild-type strain. Therefore, the reason for persistent nuclear localization of CrzA in the mutant remains unclear.

Mitochondria are essential intracellular organelles for energy production and play essential roles in buffering transient increases in cytosolic free calcium. The lack of heme A biosynthesis in the *cox10* deletion resulted in mitochondrial dysfunction in *Saccharomyces cerevisiae* (31). Meanwhile, mitochondrial membrane depolarization caused by respiratory chain defects could cause mitochondrial calcium uptake defects (49). Moreover, in fibroblasts, loss of *cox10* homologs in mammals influenced mitochondrial calcium uptake (50). These data collectively indicate that Cox10 homologs in eukaryotic organisms may all affect mitochondrial calcium uptake from the cytoplasm in cells. Our data indicate that *cox10* may contribute to Ca^{2+} uptake into mitochondria and defects in the active center of the putative farnesyltransferase Cox10 result in abnormal cellular calcium homeostasis. Previous studies showed the beneficial activities of the calcium-signaling inhibitors EGTA or FK506 in combination with the conventional antifungal agents ITC and VRC in the human fungal pathogens *C. albicans* and *A. fumigatus* through in vitro plate tests and in vivo animal model infection analysis (13, 51). This evidence underlines the relationship between the cytoplasmic calcium signaling and the drug stress response. Lastly, through antifungal susceptibility testing in all tested ITC resistant isolates, approximately half of the drug-resistant isolates having mitochondrial defects are able to be changed of drug susceptibility by reducing the enhanced cytoplasmic Ca^{2+} homeostasis. Taken together, the findings in this study are the first to demonstrate that activated calcium signaling, induced by the mitochondrial dysfunction, triggers the global overexpression of multidrug transport genes, which is a beneficial compromise strategy for surviving in a drug-stress environment.

Materials and Methods

Additional details of materials and methods can be found in *SI Appendix, SI Materials and Methods*.

Virulence assays in *G. mellonella* were performed according to Fallon et al. (52). The measurement of β-galactosidase activity was performed as previously described (53). For RNA-seq analysis, all samples were prepared and sent to perform digital transcriptome analyses by a standard RNA-seq approach (Nanjing Vazyme Co., Ltd., China). The raw Illumina sequencing data have been submitted to SRA (https://www.ncbi.nlm.nih.gov/sra) at NCBI with 6 accession numbers SRR10168714–SRR10168719. For the mitochondrial calcium measurement, a mitochondrial leading sequence obtained from cytochrome *c* oxidase Cox8 was fused with the calcium probe aequorin. Calcium transient measurements were performed as previously described (54–56). Quantitative determination of cell-wall polysaccharides was carried out as described previously (57). Mitochondrial membrane potential was detected by measurement of the accumulated rhodamine 123 by fluorescence-activated cell sorting as described in ref. 19 but with slight modifications described in *SI Appendix, SI Materials and Methods*. The intracellular drug detection by HPLC was followed the protocol as described previously (19, 58). Antifungal susceptibility testing was carried out by the broth-based microdilution method according to CLSI document M38-A2 (59). For the reactive oxygen species measurement, 2′,7′-dichlorodihydrofluorescein diacetate was used as a probe and the assay was followed as described in ref. 60.

ACKNOWLEDGMENTS. We thank Wenxia Fang (Guangxi Academy of Sciences) for kindly providing the clinical *A. fumiguatus* strains A1718 and A805; and Hong Sang (Jinling Hospital, School of Medicine, Nanjing University) for clinical *A. fumigatus* strains Afu03, Afu06, Afu07, and Afu08. This work was financially supported by the National Natural Science Foundation of China (Grants NSFC31861133014, 31370112, and 81330035) to L.L.; the Program for Jiangsu Excellent Scientific and Technological Innovation team (Grant 17CXTD00014) to L.L.; the Priority Academic Program Development (PAPD) of Jiangsu Higher Education Institutions to L.L. The funders had no role in the study.

1. B. H. Segal, Aspergillosis. *N. Engl. J. Med.* **360**, 1870–1884 (2009).
2. T. R. Dagenais, N. P. Keller, Pathogenesis of *Aspergillus fumigatus* in invasive aspergillosis. *Clin. Microbiol. Rev.* **22**, 447–465 (2009).
3. A. Abad *et al.*, What makes *Aspergillus fumigatus* a successful pathogen? Genes and molecules involved in invasive aspergillosis. *Rev. Iberoam. Micol.* **27**, 155–182 (2010).
4. T. Roemer, D. J. Krysan, Antifungal drug development: Challenges, unmet clinical needs, and new approaches. *Cold Spring Harb. Perspect. Med.* **4**, a019703 (2014).
5. D. W. Denning, M. J. Bromley, Infectious Disease. How to bolster the antifungal pipeline. *Science* **347**, 1414–1416 (2015).
6. J. W. van der Linden *et al.*, Clinical implications of azole resistance in *Aspergillus fumigatus*, The Netherlands, 2007-2009. *Emerg. Infect. Dis.* **17**, 1846–1854 (2011).
7. D. W. Denning *et al.*, Itraconazole resistance in *Aspergillus fumigatus*. *Antimicrob. Agents Chemother.* **41**, 1364–1368 (1997).
8. J. W. Slaven *et al.*, Increased expression of a novel *Aspergillus fumigatus* ABC transporter gene, *atrF*, in the presence of itraconazole in an itraconazole resistant clinical isolate. *Fungal Genet. Biol.* **36**, 199–206 (2002).
9. M. G. Fraczek *et al.*, The *cdr1B* efflux transporter is associated with non-cyp51a-mediated itraconazole resistance in *Aspergillus fumigatus*. *J. Antimicrob. Chemother.* **68**, 1486–1496 (2013).
10. L. E. Cowen *et al.*, Harnessing Hsp90 function as a powerful, broadly effective therapeutic strategy for fungal infectious disease. *Proc. Natl. Acad. Sci. U.S.A.* **106**, 2818–2823 (2009).
11. M. E. da Silva Ferreira *et al.*, *In vitro* evolution of itraconazole resistance in *Aspergillus fumigatus* involves multiple mechanisms of resistance. *Antimicrob. Agents Chemother.* **48**, 4405–4413 (2004).
12. E. Snelders *et al.*, Emergence of azole resistance in *Aspergillus fumigatus* and spread of a single resistance mechanism. *PLoS Med.* **5**, e219 (2008).
13. F. F. Liu *et al.*, Calcium signaling mediates antifungal activity of triazole drugs in the *Aspergilli*. *Fungal Genet. Biol.* **81**, 182–190 (2015).
14. R. D. Cannon *et al.*, Efflux-mediated antifungal drug resistance. *Clin. Microbiol. Rev.* **22**, 291–321 (2009).
15. M. B. Tobin, R. B. Peery, P. L. Skatrud, Genes encoding multiple drug resistance-like proteins in *Aspergillus fumigatus* and *Aspergillus flavus*. *Gene* **200**, 11–23 (1997).
16. L. E. Cowen, D. Sanglard, S. J. Howard, P. D. Rogers, D. S. Perlin, Mechanisms of antifungal drug resistance. *Cold Spring Harb. Perspect. Med.* **5**, a019752 (2014).
17. E. Snelders *et al.*, Possible environmental origin of resistance of *Aspergillus fumigatus* to medical triazoles. *Appl. Environ. Microbiol.* **75**, 4053–4057 (2009).
18. D. Hagiwara *et al.*, Non-*cyp51A* azole-resistant *Aspergillus fumigatus* isolates with mutation in HMG-CoA reductase. *Emerg. Infect. Dis.* **24**, 1889–1897 (2018).
19. X. Wei *et al.*, Screening and characterization of a non-*cyp51A* mutation in an *Aspergillus fumigatus cox10* strain conferring azole resistance. *Antimicrob. Agents Chemother.* **61**, e02101–e02116 (2016).
20. P. E. Verweij *et al.*, In-host adaptation and acquired triazole resistance in *Aspergillus fumigatus*: A dilemma for clinical management. *Lancet Infect. Dis.* **16**, e251–e260 (2016).
21. J. Meletiadis *et al.*, Differential fungicidal activities of amphotericin B and voriconazole against *Aspergillus* species determined by microbroth methodology. *Antimicrob. Agents Chemother.* **51**, 3329–3337 (2007).
22. Y. Li, Y. Zhang, L. Lu, Calcium signaling pathway is involved in non-CYP51 azole resistance in *Aspergillus fumigatus*. *Med. Mycol.* **57** (suppl. 2), S233–S238 (2019).
23. A. Butts *et al.*, Estrogen receptor antagonists are anti-cryptococcal agents that directly bind EF hand proteins and synergize with fluconazole *in vivo*. *MBio* **5**, e00765-13 (2014).
24. P. R. Juvvadi, W. J. Steinbach, Calcineurin orchestrates hyphal growth, septation, drug resistance and pathogenesis of *Aspergillus fumigatus*: Where do we go from here? *Pathogens* **4**, 883–893 (2015).
25. P. R. Juvvadi, S. C. Lee, J. Heitman, W. J. Steinbach, Calcineurin in fungal virulence and drug resistance: Prospects for harnessing targeted inhibition of calcineurin for an antifungal therapeutic approach. *Virulence* **8**, 186–197 (2017).
26. D. S. Perlin, E. Shor, Y. Zhao, Update on antifungal drug resistance. *Curr. Clin. Microbiol. Rep.* **2**, 84–95 (2015).
27. P. R. Juvvadi *et al.*, Calcium-Mediated induction of paradoxical growth following caspofungin treatment is associated with calcineurin activation and phosphorylation in *Aspergillus fumigatus*. *Antimicrob. Agents Chemother.* **59**, 4946–4955 (2015).
28. V. Y. Ganitkevich, The role of mitochondria in cytoplasmic Ca^{2+} cycling. *Exp. Physiol.* **88**, 91–97 (2003).
29. H. J. Kim, O. Khalimonchuk, P. M. Smith, D. R. Winge, Structure, function, and assembly of heme centers in mitochondrial respiratory complexes. *Biochim. Biophys. Acta* **1823**, 1604–1616 (2012).
30. H. Fukui, F. Diaz, S. Garcia, C. T. Moraes, Cytochrome c oxidase deficiency in neurons decreases both oxidative stress and amyloid formation in a mouse model of Alzheimer's disease. *Proc. Natl. Acad. Sci. U.S.A.* **104**, 14163–14168 (2007).
31. M. Bestwick, O. Khalimonchuk, F. Pierrel, D. R. Winge, The role of Coa2 in hemylation of yeast Cox1 revealed by its genetic interaction with Cox10. *Mol. Cell. Biol.* **30**, 172–185 (2010).
32. T. C. Hallstrom, W. S. Moye-Rowley, Multiple signals from dysfunctional mitochondria activate the pleiotropic drug resistance pathway in *Saccharomyces cerevisiae*. *J. Biol. Chem.* **275**, 37347–37356 (2000).
33. M. Neubauer *et al.*, Mitochondrial dynamics in the pathogenic mold *Aspergillus fumigatus*: Therapeutic and evolutionary implications. *Mol. Microbiol.* **98**, 930–945 (2015).
34. B. Bareth *et al.*, The heme a synthase Cox15 associates with cytochrome c oxidase assembly intermediates during Cox1 maturation. *Mol. Cell. Biol.* **33**, 4128–4137 (2013).
35. A. Baracca, G. Sgarbi, G. Solaini, G. Lenaz, Rhodamine 123 as a probe of mitochondrial membrane potential: Evaluation of proton flux through $F_{(0)}$ during ATP synthesis. *Biochim. Biophys. Acta* **1606**, 137–146 (2003).
36. E. G. Demers *et al.*, Evolution of drug resistance in an antifungal-naive chronic *Candida lusitaniae* infection. *Proc. Natl. Acad. Sci. U.S.A.* **115**, 12040–12045 (2018).
37. M. Shingu-Vazquez, A. Traven, Mitochondria and fungal pathogenesis: Drug tolerance, virulence, and potential for antifungal therapy. *Eukaryot. Cell* **10**, 1376–1383 (2011).

38. D. E. Clapham, Calcium signaling. *Cell* **131**, 1047–1058 (2007).
39. G. Nelson *et al*., Calcium measurement in living filamentous fungi expressing codon-optimized aequorin. *Mol. Microbiol.* **52**, 1437–1450 (2004).
40. P. R. Juvvadi, F. Lamoth, W. J. Steinbach, Calcineurin as a multifunctional regulator: Unraveling novel functions in fungal stress responses, hyphal growth, drug resistance, and pathogenesis. *Fungal Biol. Rev.* **28**, 56–69 (2014).
41. J. B. Anderson, Evolution of antifungal-drug resistance: Mechanisms and pathogen fitness. *Nat. Rev. Microbiol.* **3**, 547–556 (2005).
42. F. L. van de Veerdonk, M. S. Gresnigt, L. Romani, M. G. Netea, J. P. Latgé, *Aspergillus fumigatus* morphology and dynamic host interactions. *Nat. Rev. Microbiol.* **15**, 661–674 (2017).
43. R. S. Shapiro, N. Robbins, L. E. Cowen, Regulatory circuitry governing fungal development, drug resistance, and disease. *Microbiol. Mol. Biol. Rev.* **75**, 213–267 (2011).
44. C. Sharma, S. Nelson-Sathi, A. Singh, M. Radhakrishna Pillai, A. Chowdhary, Genomic perspective of triazole resistance in clinical and environmental *Aspergillus fumigatus* isolates without *cyp51A* mutations. *Fungal Genet. Biol.* **132**, 103265 (2019).
45. P. Belenky, D. Camacho, J. J. Collins, Fungicidal drugs induce a common oxidative-damage cellular death pathway. *Cell Rep.* **3**, 350–358 (2013).
46. E. Shekhova, O. Kniemeyer, A. A. Brakhage, Induction of mitochondrial reactive oxygen species production by itraconazole, terbinafine, and amphotericin B as a mode of action against *Aspergillus fumigatus*. *Antimicrob. Agents Chemother.* **61**, e00978-17 (2017).
47. D. J. Dwyer, M. A. Kohanski, J. J. Collins, Role of reactive oxygen species in antibiotic action and resistance. *Curr. Opin. Microbiol.* **12**, 482–489 (2009).
48. L. N. A. Ries *et al*., The *Aspergillus fumigatus* CrzA transcription factor activates chitin synthase gene expression during the caspofungin paradoxical effect. *MBio* **8**, e00705–e00717 (2017).
49. D. G. Nicholls, M. W. Ward, Mitochondrial membrane potential and neuronal glutamate excitotoxicity: Mortality and millivolts. *Trends Neurosci.* **23**, 166–174 (2000).
50. V. Paupe, J. Prudent, E. P. Dassa, O. Z. Rendon, E. A. Shoubridge, CCDC90A (MCUR1) is a cytochrome c oxidase assembly factor and not a regulator of the mitochondrial calcium uniporter. *Cell Metab.* **21**, 109–116 (2015).
51. I. I. Raad *et al*., Role of ethylene diamine tetra-acetic acid (EDTA) in catheter lock solutions: EDTA enhances the antifungal activity of amphotericin B lipid complex against *Candida* embedded in biofilm. *Int. J. Antimicrob. Agents* **32**, 515–518 (2008).
52. J. P. Fallon, N. Troy, K. Kavanagh, Pre-exposure of *Galleria mellonella* larvae to different doses of *Aspergillus fumigatus* conidia causes differential activation of cellular and humoral immune responses. *Virulence* **2**, 413–421 (2011).
53. T. J. Schoberle *et al*., A novel C2H2 transcription factor that regulates gliA expression interdependently with GliZ in *Aspergillus fumigatus*. *PLoS Genet.* **10**, e1004336 (2014).
54. Y. Zhang *et al*., Palmitoylation of the cysteine residue in the DHHC motif of a palmitoyl transferase mediates Ca^{2+} homeostasis in *Aspergillus*. *PLoS Genet.* **12**, e1005977 (2016).
55. V. Greene, H. Cao, F. A. Schanne, D. C. Bartelt, Oxidative stress-induced calcium signalling in *Aspergillus nidulans*. *Cell. Signal.* **14**, 437–443 (2002).
56. R. Rizzuto, A. W. Simpson, M. Brini, T. Pozzan, Rapid changes of mitochondrial Ca^{2+} revealed by specifically targeted recombinant aequorin. *Nature* **358**, 325–327 (1992).
57. J. M. François, A simple method for quantitative determination of polysaccharides in fungal cell walls. *Nat. Protoc.* **1**, 2995–3000 (2006).
58. E. Cendejas-Bueno, M. Cuenca-Estrella, A. Gomez-Lopez, A simple, sensitive HPLC-PDA method for the quantification of itraconazole and hydroxy itraconazole in human serum: A reference laboratory experience. *Diagn. Microbiol. Infect. Dis.* **76**, 314–320 (2013).
59. C. L. S. Institute, "Reference method for broth dilution antifungal susceptibility testing of filamentous fungi; approved standard—2nd ed" (CLSI document M38-A2, Clinical and Laboratory Standards Institute, Wayne, PA, 2008).
60. L. Li *et al*., Genetic dissection of a mitochondria-vacuole signaling pathway in yeast reveals a link between chronic oxidative stress and vacuolar iron transport. *J. Biol. Chem.* **285**, 10232–10242 (2010).